IEEE Access
Multidisciplinary ⋮ Rapid Review ⋮ Open Access Journal

Received 1 April 2024, accepted 12 April 2024, date of publication 17 April 2024, date of current version 24 April 2024.

Digital Object Identifier 10.1109/ACCESS.2024.3390091

RESEARCH ARTICLE

Zero-Pole Cancellation Based Iterative Learning Control Method for Speed Ripple Suppression of Single Rolling Rotor Compressor

YAN WANG[1], SHENGHUI DENG[1], AND WENQI LU[2], (Member, IEEE)
[1]College of Information Science and Engineering, Zhejiang Sci-Tech University, Hangzhou 310018, China
[2]College of Mechanical Engineering, Zhejiang Sci-Tech University, Hangzhou 310018, China

Corresponding author: Yan Wang (wangyan2021@zstu.edu.cn)

This work was supported in part by the National Natural Science Foundation of China under Grant 52277068; and in part by the Key Research and Development Program of Zhejiang Science and Technology Department under Grant 2024C01230, Grant 2023C01159, and Grant 2022C01242.

ABSTRACT Owing to the severe load torque fluctuation, the speed ripple is a significant concern for the compressor drive system, especially within low frequency range. To address this issue, a zero-pole cancellation (ZPC) based iterative learning control (ILC) method is proposed for speed ripple suppression in this paper. The load torque characteristic is obtained based on the estimated speed harmonics. The essence of the speed ripple is investigated utilizing the compressor mechanical model, which attributes to the conjugate poles effect of the load torque term at the specific mechanical frequency. The zero point of the conventional ILC method is fixed at s=0, which can hardly reduce the dominant poles effect of the torque term. Afterwards, the poles' matching function is analytically derived to cancel out the dominant poles of the torque term, and then the specific order harmonic can be effectively suppressed. Considering the non-periodic disturbance caused by the operating frequency and temperature variation, the error correction law is designed to avoid the error accumulation and ensure the performance of proposed ILC method. Finally, the effectiveness of the method is validated by experiments through a 750W compressor drive system. Experimental results indicate that the total speed ripples reduce by nearly 60% and each harmonic component of the speed ripple can be effectively suppressed according to the FFT results.

INDEX TERMS PMSM-compressor drive, torque ripple, iterative learning control, speed harmonics.

I. INTRODUCTION

Owing to high power density, efficiency and wide speed range, the permanent magnet synchronous motor (PMSM) has been popular in electric vehicles, electric aircrafts and household appliances [1], [2], [3]. Compared with the reciprocating compressor, the PMSM based single rolling rotor compressor is commonly used in the air conditioner system due to low vibration and fewer piston parts. In general, the compressor is sealed inside the compression cylinder filled with refrigerant and the hall sensors or encoders will fail to acquire the position or speed information [4], [5], [6]. Influenced by the eccentric placement of the rotor and the as shown in FIGURE 1, where the friction always exists between the slider and rotor during the compressor operation process. The rotor is linked with the motor through the crankshaft, and the closed volume continues to shrink as the crankshaft rotates, which results in the high refrigerant pressure. The discharge process will continue as the pressure reaching the exhaust point. Therefore, the periodic load torque varies with refrigerant pressure and easily leads to unstable operation, which is still a significant concern limiting the dynamic performance of the compressor.

The torque ripple is mainly investigated form aspects such as motor design, control effects of the inverter, and inherent load characteristic considering the specific application.

The associate editor coordinating the review of this manuscript and approving it for publication was Santi C. Pavone.

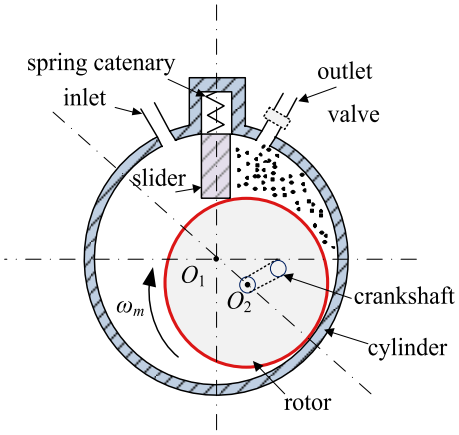

FIGURE 1. Structure of the single rolling rotor compressor section part.

The average torque and torque ripple are analyzed from the motor structure in [7], harmonics of motor flux and cogging torque also produce periodic disturbance and is independent of the stator current [8], the torque ripple caused by the rotor position error in [9] is analytically discussed. In addition, the change in hardware topology with reduced DC-link capacitor will leads to periodic speed ripple synchronized with the fluctuated DC-link voltage [10], [11]. Therefore, the torque ripple is inevitable both during the motor design stage or motor control stage. The compressor in the air-conditioner repeats the process of inhaling, compression and exhausting to circulate the refrigerant. The pressure difference between the input and output of the copper pipe contributes to complex characteristic of the load torque, which results in periodic speed ripple and is different from that in [7], [8], [9], [10], and [11]. On account of different factors of torque or speed ripple, many researchers dedicated to reducing the speed ripple through motor design and inverter control. For the motor design stage, the shifting angle of permanent magnet (PM) and open angle of air barriers are introduced to reduce the torque ripple in [7], the comparison between the shaped PMs and conventional tile PMs are discussed from aspects of torque ripple and average torque [12], whereas the latter mainly focuses on the motor current modification to improve the speed ripple. The source of torque ripple from harmonics of rotor flux, cogging torque, and dead-band time of inverter are modeled in [8], where a proportional-integral-resonant (PIR) controller is adopted in both current and speed loop considering the optimal phase adjustment. A generalized torque ripple model produced by the rotor position error is deduced in [9], and a compensation algorithm is proposed based on the non-idealities of the rotor position sensor. The of harmonic current are optimized by several algorithms such as the least mean square based adaptive filter [13] or genetic algorithm [14] based on the torque model of the PMSM, where the harmonics of stator voltage, stator current and PM flux linkage are included.

In summary, the above-mentioned methods are based on the motor electrical model, where the accurate motor parameters or optimization algorithms are used to achieve accurate torque ripple predication. However, the characteristic of the load torque itself is easily ignored under this condition especially for some specific applications, and the overall cost is another concern since the complex harmonic current design which depends on the high-performance controller. From another aspect, the torque ripple can be clearly reflected in the motor speed which seems to be result of the torque ripple [11], [15], [16], [17]. Therefore, the result-to-reason prospect is investigated and the speed ripple should be analytically modeled first. Both the torque and speed ripples are linked through the mechanical/motion model; thus, the mechanical model-based approach is developed to reduce speed ripple. Two iterative learning control (ILC) strategies in time and frequency domain are compared to minimize the periodic speed ripples caused by torque pulsation in [15] from the equation of the motor dynamic. A closed-loop fuzzy-logic current controller with the magnitude of the speed harmonic feedback is proposed in [16], accurate motor parameters and nonlinearity of the drive are avoided. The torque observer and iterative learning controller are designed for the reduced DC-link capacitor motor drive, the speed ripple related to load torque and DC-link voltage fluctuation are observed and compensated by closed-loop structure [17]. Based on the result-to-reason prospect, the torque disturbance can be extracted from the speed ripple with the corresponding component, which is independent of the motor electrical model. The ILC method is generally used to track the repetitive or periodic system with a fixed period by iterating the previous signal, which is in parallel with the proportional-integral (PI) speed controller to generate the current reference [18], [19]. However, the fundamental is the main component of the load torque for single rolling rotor compressor, which can be obtained first to enhance the iteration effect. On account of the load torque characteristic considering the operating frequency and temperature variation, the error accumulation of the iteration process should be addressed, which easily induces the offset and output saturation.

To solve the problem, an improved ILC based on zero-pole cancellation (ZPC) method is proposed, the essence of the speed ripple has been investigated through the compressor motion model. Then, the poles' matching function is proposed to weaken the dominant poles effect of the torque term and suppress the specific order harmonic. Also, the error correction law aims to be derived to remove the influence of the non-periodic signal. Compared with the previous studies, the contributions in this paper can be summarized as follows:

(1) The compressor motion model is presented free of PMSM parameters, based on which, the essence of the speed ripple is investigated that the mismatch between the zeros of conventional ILC and the conjugate poles of the load torque.

(2) The poles' matching function is analytically derived to reduce the dominant poles effect of the torque term, which effectively suppress the specific order harmonic according to the sample data by the pre-designed experiments.

(3) To deal with the non-periodic disturbance caused by the operating frequency and temperature variation for the compressor system, the error correction law is proposed to enhance the performance of the conventional ILC.

This paper is organized as follows. In Section II, the PMSM based compressor drive is analyzed from aspects of sensorless control strategy and load torque characteristics in detail. The problems of the conventional ILC are introduced in Section III and an improved ILC based on zero-pole cancellation method is addressed. The experimental results are presented in Section IV to validate the effectiveness of the proposed method and the conclusion is summarized in Section V.

II. ANALYSIS OF PMSM BASED COMPRESSOR DRIVE

A. SENSORLESS STRATEGY WITH LINEAR STATE OBSERVER

The single-phase input PMSM compressor drive used in air-conditioner system is shown in FIGURE. 2, where the DC-link voltage is obtained from the grid through an uncontrolled diode rectifier. The PMSM compressor is driven by a three-phase inverter with the intelligent power module, where the compressor is sealed in the cylinder full of refrigerant and is difficult to install the position sensors. In addition, the compressor drives of which are low cost systems in household appliances and the sensorless control strategy is applied to ensure the electrical angle acquisition [4], [20], [21].

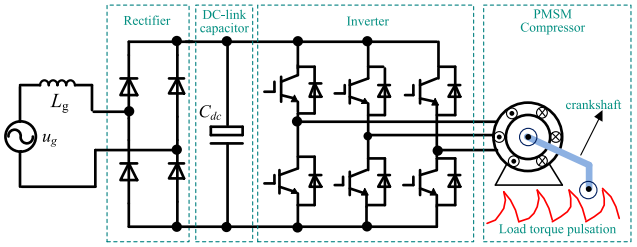

FIGURE 2. Single phase input IPMSM compressor drive.

The speed ripple is an inevitable problem due to load torque pulsation when the compressor operating in low frequency range. In order to improve the performance of the compressor drive, an effective speed ripple suppression strategy is carried out, which depends on the accurate position estimation approach. The field-oriented control with a linear state observer used to obtain the compressor speed and position is implemented, which ensures the position error converge to zero.

Different frames are shown in FIGURE 3 to illustrate the relationship between the estimated and real component (i.e., the relationship of motor d-q frame and estimated synchronous γ-δ frame), where the α-β frame is fixed on the stator winding while the d-q and γ-δ frame is rotating with the permanent magnet.

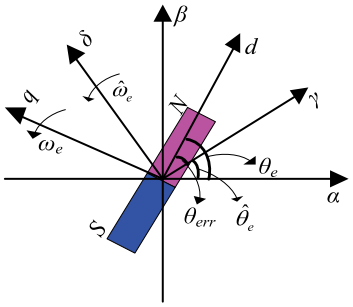

FIGURE 3. Relationship between different reference frames.

The voltage equation in d-q frame with the electrical angular velocity ω_e is given as follows

$$\begin{cases} u_d = R_s i_d + L_d \dfrac{di_d}{dt} - \omega_e L_q i_q \\ u_q = R_s i_q + L_q \dfrac{di_q}{dt} + \omega_e L_d i_d + \omega_e \psi_f \end{cases} \tag{1}$$

where u_d, u_q, i_d, i_q, L_d, L_q are the d-axis and q-axis voltage, current and inductance, respectively. R_s and ψ_f is the winding resistance and permanent flux linkage.

In order to obtain the rotor position, the mathematical model is established in estimated synchronous γ-δ frame with the angular velocity $\hat{\omega}_e$. As is illustrated in FIGURE 3, the γ-δ frame lags the d-q frame of the estimated error θ_{err}. Then the voltage equation in (1) can be transformed into estimated synchronous γ-δ frame as follows

$$\begin{cases} u_\gamma = R_s i_\gamma + L_d \dfrac{di_\gamma}{dt} - \hat{\omega}_e L_q i_\delta + e_\gamma \\ u_\delta = R_s i_\delta + L_q \dfrac{di_\delta}{dt} + \hat{\omega}_e L_d i_d + e_\delta \end{cases} \tag{2}$$

where the variables are denoted with the subscript γ-δ, e_γ and e_δ represent the motor back electromotive force (EMF) due to the position error, which can be presented as

$$\begin{cases} e_\gamma = -\omega_e \psi_f \sin\theta_{err} \\ e_\delta = \omega_e \psi_f \cos\theta_{err} \end{cases} \tag{3}$$

Both e_γ and e_δ contains the information of estimated error, it can be seen in (3) that the back EMF terms are neither outputs nor inputs of the system. Therefore, a linear state space model is applied assuming that the motor speed and position remain constant during the control period. The state variables e_γ and e_δ meet the following requirement as

$$\begin{cases} \dot{e}_\gamma = 0 \\ \dot{e}_\delta = 0 \end{cases} \tag{4}$$

Combing (2) and (4), the estimation model in the γ-δ frame can be presented as follows

$$\begin{cases} \dot{\mathbf{x}} = \mathbf{A}\mathbf{x} + \mathbf{B}\mathbf{u} \\ \dot{\mathbf{y}} = \mathbf{C}\mathbf{x} \end{cases} \tag{5}$$

where $\boldsymbol{i} = [i_\gamma, i_\delta, e_\gamma, e_\delta]^T$, $\boldsymbol{u} = [u_\gamma, u_\delta]^T$, $\boldsymbol{y} = [i_\gamma, i_\delta]^T$, the coefficient matrixes are given in detail in Appendix.

A linear observer with the current feedback is established as follows

$$\dot{\hat{\mathbf{x}}} = \mathbf{A}\hat{\mathbf{x}} + \mathbf{B}\mathbf{u} + \mathbf{M}\left(\mathbf{y} - \mathbf{C}\hat{\mathbf{x}}\right) \tag{6}$$

where $\mathbf{M}$ is the feedback gain matrix and the superscript hat denotes estimated variables.

Then, the state error equation can be derived as

$$\dot{\tilde{\mathbf{x}}} = \mathbf{A}\tilde{\mathbf{x}} - \mathbf{M}\mathbf{C}\tilde{\mathbf{x}} = (\mathbf{A} - \mathbf{M}\mathbf{C})\,\tilde{\mathbf{x}} \tag{7}$$

The convergence and dynamic response of the observer depend on the characteristics of the matrix (**A**-**MC**), to maintain the system stability and fast convergence of the state error, the poles placement method is applied to determine the elements of feedback gain matrix. Then, the Laplace transformation is implemented on (7) as follows

$$\tilde{\mathbf{x}}(s) = (s\mathbf{I} - \mathbf{A} + \mathbf{M}\mathbf{C})^{-1}\,\tilde{\mathbf{x}}(0) \tag{8}$$

Since the state variables in (5) are consistent on the time dimension, all the four poles can be selected on the negative real axis to improve the dynamic response and simplify the calculation process, which can be defined as the bandwidth of the observer and the constraint can be given as

$$\det(s\mathbf{I} - \mathbf{A} + \mathbf{M}\mathbf{C}) = (s + \omega_b)^4 \tag{9}$$

Then the feedback gain matrix $\mathbf{M}$ can be calculated as follows

$$\mathbf{M} = \begin{bmatrix} 2\omega_b - \dfrac{R_s}{L_d} & -\hat{\omega}_e\dfrac{L_d}{L_q} & \omega_b^2 L_d & 0 \\ \hat{\omega}_e\dfrac{L_q}{L_d} & 2\omega_b - \dfrac{R_s}{L_q} & 0 & \omega_b^2 L_q \end{bmatrix}^T \tag{10}$$

The back EMF e_γ and e_δ is obtained with the observer (6), and hence the position error can be derived with the terms as follows

$$\theta_{err} = -ac\tan\frac{e_\gamma}{e_\delta} \cong -\frac{e_\gamma}{e_\delta} \tag{11}$$

To avoid the inverse trigonometric function calculation in the controller and achieve the precise tracking performance, the phase lock loop (PLL) structure is applied to reduce the estimated error between the γ-δ and d-q frame in FIGURE 4.

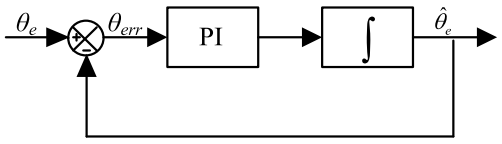

FIGURE 4. Control block of PLL based rotor position estimation.

The PI unit is used to regulate θ_{err} and the output is the estimated angular velocity $\hat{\omega}_e$. Then, the rotor position can be achieved through the integration of $\hat{\omega}_e$. In summary, the whole control scheme of the linear state space observer is presented in FIGURE 5.

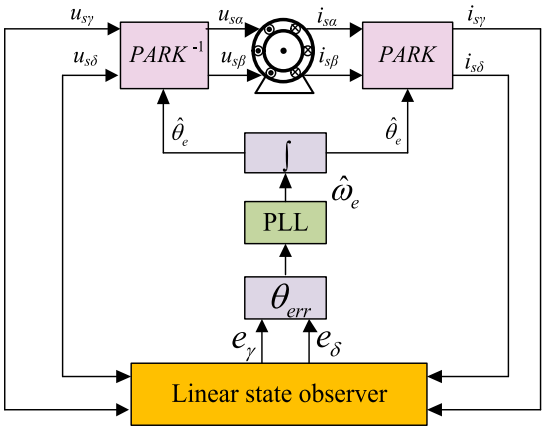

FIGURE 5. The whole control scheme of the linear state space observer for position estimation.

B. LOAD TORQUE ANALYSIS BASED ON SPEED RIPPLE

Due to the special crankshaft design for the single rolling rotor compressor, both the suction compression and exhaust process appear within a given cycle as shown in FIGURE 6, which results in the variation of pressure and volume for the refrigerant, and hence the amplitude of the torque ripple varies with the rotor mechanical position and depends on the temperature condition and refrigerant pressure.

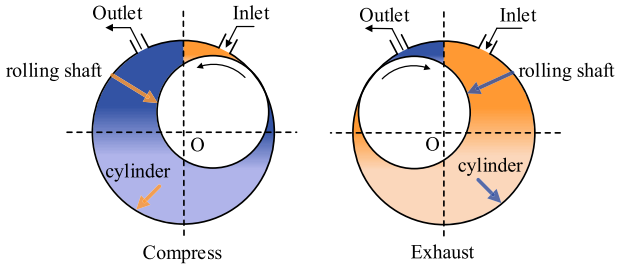

FIGURE 6. Process of compress and exhaust during a mechanical cycle.

According to the sample data by the pre-designed experiments, FIGURE 7 shows the load torque characteristics under different cases, it can be seen that the periodic pulsations exist in each mechanical period from 0 to 360 degree, and the maximum fluctuations for each case is different. The load torque seriously fluctuates due to the pressure difference between the inlet and outlet especially when the compressor operating under low frequency range (compressor speed between 600∼1500rpm).

The load torque characteristics shown in FIGURE 7 are irregular within the period, however, which can be considered as the superposition of sine waves with Fourier series as

$$T_L(t) = T_{L0} + \sum_{k=1}^{\infty} T_{Lk}\sin(k\omega_m t + \varphi_k) \tag{12}$$

where T_L is the load torque, T_{L0} is the dc component, T_{Lk} and φ_k is the amplitude and phase of the harmonic

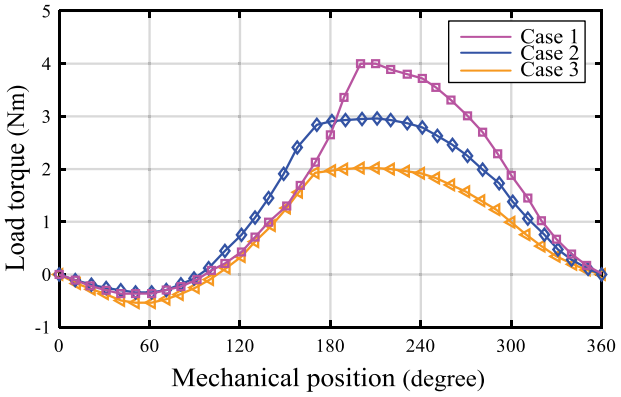

FIGURE 7. Characteristics of load torque under different cases.

component. The k^{th} harmonic component is multi-times of the compressor mechanical frequency ω_m. To further analyze the characteristics of load torque in FIGURE 8, the FFT result of case 2 is presented when the compressor operating with frequency of 20 Hz, it can be seen that both the dc and fundamental components are the main terms for the periodic load torque, while the other terms in (12) are relatively small.

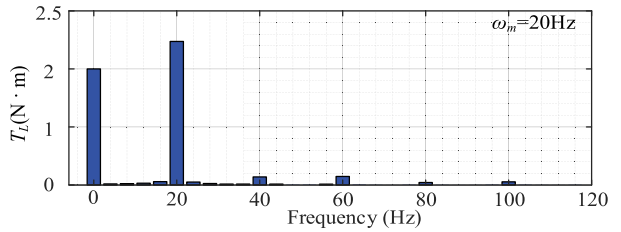

FIGURE 8. FFT result of the load torque component of $\omega_m = 20$Hz.

Applying the Laplace transformation on (12) and the load torque $T_L(s)$ can be obtained as

$$T_L(s) = T_{L0} + \sum_{k=1}^{+\infty} T_{Lk}(s) \tag{13}$$

where the harmonic component can be calculated as

$$\begin{aligned} T_{Lk}(s) &= \int_{0-}^{\infty} T_{Lk} \left(\sin\left(k\omega_m t\right)\cos\varphi_k + \cos\left(k\omega_m t\right)\sin\varphi_k\right) e^{-st}\,dt \\ &= T_{Lk}\frac{s\sin\varphi_k + k\omega_m\cos\varphi_k}{s^2 + (k\omega_m)^2} \end{aligned} \tag{14}$$

The equation of the compressor dynamics can be described as

$$J_m\frac{d\omega_m}{dt} = T_e - T_L - B_m\omega_m \tag{15}$$

where J_m, T_e and B_m are the mechanical inertia, compressor electromagnetic torque and frictional coefficient, respectively. Combing (13), (14) and (15), the constant and ripple components of the motor speed can be derived as (16). The frictional torque term can be ignored when the compressor operating within low frequency range.

$$\begin{aligned} \omega_m(s) &= \omega_{m0}(s) + \omega_{mk}(s) \\ &= \frac{1}{J_m}\left(\underbrace{\frac{T_e - T_{L0}}{s}}_{\text{constant}} - \underbrace{\frac{T_{Lk}}{s}\frac{s\sin\varphi_k + k\omega_m\cos\varphi_k}{s^2 + (k\omega_m)^2}}_{\text{ripple}}\right) \end{aligned} \tag{16}$$

It can be seen in (16) that the harmonic components of speed ripple are the same order with that of load torque, which indicates the load torque ripple can be clearly reflected in the motor speed ripple through the mechanical model. According to (16), the speed ripple is more susceptible under lower frequency. Therefore, the research mainly focuses on the fundamental component of the speed ripple, which has been analyzed in FIGURE 8.

III. PROPOSED METHODS

A. PRINCIPLE OF SPEED RIPPLE SUPPRESSION

The control block diagram of the speed ripple suppression for the compressor is shown in FIGURE 9, where the feedforward controller paralleled with the speed controller is employed to generate the compensation current. It can be concluded that the q-axis reference current can be divided into two parts, one is the output of the speed controller to track the dc component, while the other i_{qc} mainly contains the ac component for ripple suppression.

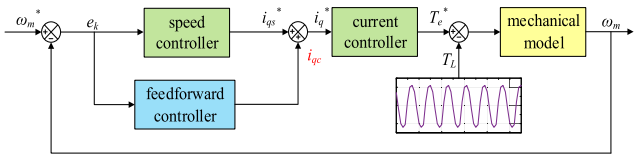

FIGURE 9. The control block diagram of the speed ripple suppression.

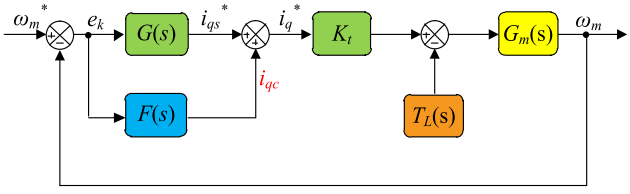

FIGURE 10. Simplified control loop based on the mechanical model.

To derive the transfer function of ω_m(s) in the frequency domain, the control loop based on the mechanical model can be simplified in FIGURE 10, where $G(s)$ represents the speed controller and K_t can be regarded as the equivalent torque coefficient of the current controller in the low frequency range. $G_m(s)$ is the mechanical model and can be presented as

$$G_m(s) = \frac{1}{J_m s + B_m} \tag{17}$$

According to FIGURE 10, the transfer function of ω_m(s) considering the disturbance of the load torque can be presented as

$$\omega_m(s) = \underbrace{R(s)\omega_m^*(s)}_{\omega_{mr}(s)} + \underbrace{D(s)T_L(s)}_{\omega_{md}(s)} \tag{18}$$

where $R(s)$ and $D(s)$ are the reference tracking and disturbance transfer function, respectively. The disturbance term caused by the load torque can be derived as

$$\omega_{md}(s) = D(s)T_L(s) = \frac{-G_m(s)}{1 + K_t G_m(s)\,(G(s) + F(s))} T_L(s) \tag{19}$$

For the general control system ignoring the disturbance rejection (i.e., F(s)=0), the amplitude of the disturbance term can be derived as

$$\begin{aligned} |\omega_{md}(j\omega)|_{F(j\omega)=0} &= |D(j\omega)T_L(j\omega)| \\ &= \frac{|T_L(j\omega)|}{|J_m\omega + B_m| + K_t\left|K_{sp} + \frac{K_{si}}{j\omega}\right|} \end{aligned} \tag{20}$$

where K_{sp} and K_{si} are the proportional and integral gain of the speed controller. It can be seen in (20) that the value of $|\omega_{md}(j\omega)|$ mainly depends on the mechanical inertia and PI unit gains. However, the PI unit is applied for regulating the error for higher tracking performance, which is limited to the maximum mechanical acceleration of the compressor structure. Therefore, the extra unit should be added to deal with the speed ripple caused by the disturbance, especially the typical periodic load torque characteristic of the compressor, which can be analyzed in detail according to different types of $F(s)$.

B. PD-TYPE ITERATIVE LEARNING CONTROLLER BASED METHOD

The proportional-differential (PD) type iterative learning control (ILC) method is common for speed ripple suppression and the specific structure is shown in FIGURE 11, which consists of PD part and iteration part.

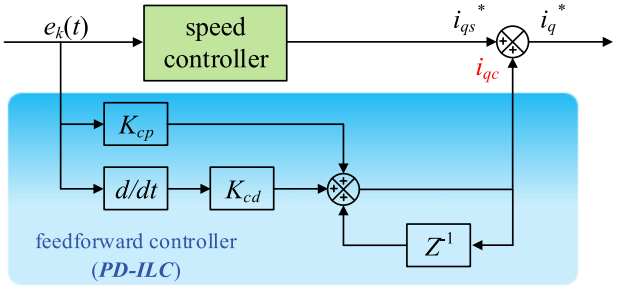

FIGURE 11. The specific structure of ILC controller.

The output is feedforward on the speed controller to generate the q-axis reference current and can be expressed as

$$i_{qc}(t) = i_{qc(k-1)}(t) + K_{cp}e(t) + K_{cd}[e(t) - e_{k-1}(t)] \tag{21}$$

where K_{cp} and K_{cd} are the gain of the proportional and differential unit. The PD type ILC method in FIGURE 11 can be derived with the backward Euler method as follows

$$F(s)_{PD-ILC} = \frac{K_{cp} + K_{cd}sT_s}{sT_s} \tag{22}$$

Combing (19), (21) and (22), the load torque disturbance transfer function can be rewritten as

$$D(s) = \frac{-sT_s}{s^2J_mT_s + sK_tT_s(K_{sp} + K_{cd}) + K_t(K_{si}T_s + K_{cp})} \tag{23}$$

It can be seen in (23) that the zero $s = 0$ is included in $D(s)$ when the conventional ILC is applied. In order to investigate the principle of the speed ripple suppression, both the poles and zeros of $T_L(s)$ and $D(s)$ are illustrated in FIGURE 12. It can be seen in FIGURE 12(a) that a pair of poles are included in $T_L(s)$ while the zero of $D(s)$ is fixed at $s = 0$, which is consistent with (14) and (23), respectively. Therefore, the effect of the poles of $T_L(s)$ can be hardly eliminated and the performance of speed ripple suppression is poor. Inspired by this, an extra pair of zeros can be induced by the designed $F(s)$ as shown in FIGURE 10(b). The poles effect of $T_L(s)$ can be weakened as the zeros gradually move closely according to the zero-pole cancellation principle. Therefore, the speed ripple can be effectively suppressed with the reasonable zero configuration with a certain bandwidth.

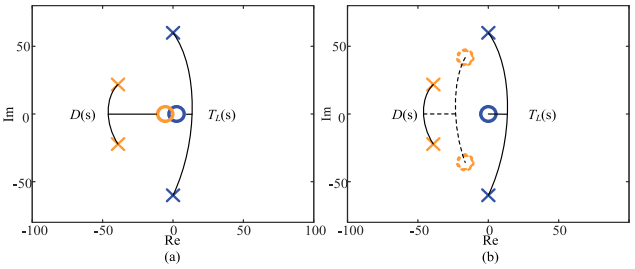

FIGURE 12. The poles and zeros of the disturbance term. (a) Without the feedforward controller. (b) With the conventional ILC controller.

In addition, considering the mechanical structure and temperature variation for the compressor system, the feedforward current error will be accumulated due to the iteration process, which will further limit the performance of conventional ILC method or causes the saturation of the controller.

C. PROPOSED SPEED RIPPLE SUPPRESSION METHOD BASED ON ZERO-POLE CANCELLATION

On account of the poor effect of conventional ILC method and the concern of error accumulation, an improved iterative learning controller based on zero-pole cancellation (ZPC) method is addressed in this section, which can be divided into two parts, one is the poles matching function to suppress the specific frequency terms and the other is the error correction law to avoid the accumulation of feedforward current error. The detailed control block diagram is presented in

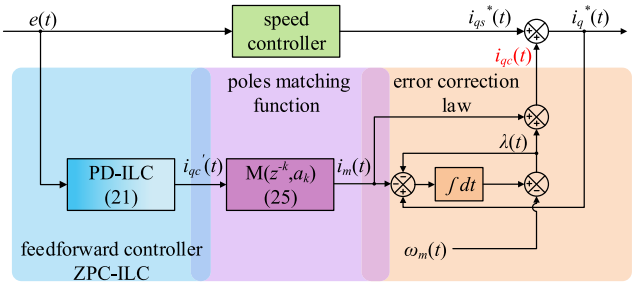

FIGURE 13. Control block diagram of the proposed speed ripple suppression method.

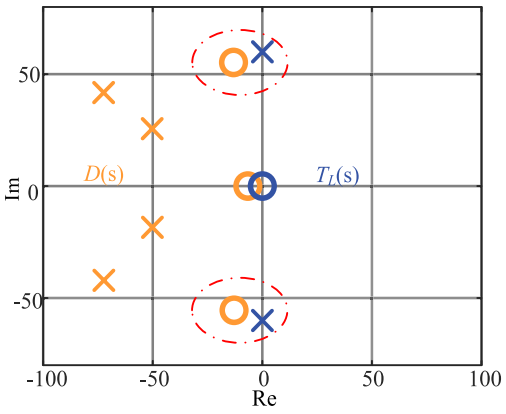

FIGURE 14. The poles and zeros of the disturbance term with the proposed method.

FIGURE 13, from which it can be seen that the output of the ILC is filtered by the poles matching function, and then the error correction law is applied to remove the non-periodic disturbance to prevent the controller saturation.

Compared with the conventional ILC method in (21), the q-axis current reference of the proposed method can be expressed as

$$\begin{cases} i'_{qc}(t) = i_{qc(k-1)}(t) + K_{cp}e(t) + K_{cd}[e(t) - e_{k-1}(t)] \\ i_m(t) = M(z^{-k}, \alpha_k)i'_{qc}(t) \\ \lambda(t) = \int \left(i_q^*(t) - i_m(t) - \lambda(t)\right)dt - \omega_m(t) \\ i_{qc}(t) = \lambda(t) + i_m(t) \end{cases} \tag{24}$$

The poles' matching function is mainly applied to extract the fundamental component of the feedforward current and decline the effect of disturbance term from zero-pole cancellation principle, which is cascade with the ILC as shown in FIGURE 13. According to (14), two poles $s = \pm j\omega_m$ are included in the fundamental term of the load torque, so that the poles matching function can be designed as

$$M(z^{-k}, \alpha_k) = \frac{1 - z^{-1}}{1 - \alpha_1 z^{-1} - \alpha_2 z^{-2}} \tag{25}$$

where α_1 and α_2 are the coefficients and will be discussed in the following section. According to (24), the feedforward controller can be derived as follow (26) while ignoring the error correction law.

$$F(s) = \frac{K_{cp} + K_{cd}sT_s}{-\alpha_2 T_s^2 s^2 + (2\alpha_2 + \alpha_1)T_s s + 1 - \alpha_1 - \alpha_2} \tag{26}$$

Combing (19), (24) and (26), the load torque disturbance transfer function can be rewritten as where D_1 and D_2 are the coefficients, which are formulated in Appendix. According to (27), as shown at the bottom of the next page, a pair of conjugate zeros are included in $D(s)$ comparing with that in (23), and the effect of zero-pole cancellation are illustrated in FIGURE 14.

When the poles' matching function is embedded, it can be observed that a pair of conjugate zeros provided by the disturbance transfer function gradually move to the poles of load torque term $T_L(s)$. Therefore, the speed ripple can be suppressed due to the reduced effect for the poles of $T_L(s)$.

Considering the numerator of (27) with the zero $s = 0$, the remaining part can be considered as a typical 2nd order system with the damping frequency ω_d, which ensures the certain bandwidth even if the poles' movement. The model can be presented as follows

$$\begin{aligned} N(s) &= -\alpha_2 T_s^2 s^2 + (2\alpha_2 + \alpha_1)T_s s + 1 - \alpha_1 - \alpha_2 \\ &= s^2 + 2\omega_d T_s s + \omega_t^2 \end{aligned} \tag{28}$$

where ω_t is the natural frequency. Then the coefficients α_1 and α_2 can be determined as

$$\begin{cases} \alpha_1 = \dfrac{2\left(\omega_d T_s^2 + 1\right)}{\left(2\omega_d + \omega_t^2\right)T_s^2 + 1} \\ \alpha_2 = \dfrac{-1}{\left(2\omega_d + \omega_t^2\right)T_s^2 + 1} \end{cases} \tag{29}$$

FIGURE 15 shows the relationship of α_1 and α_2 between ω_t and ω_d, respectively. It can be seen that α_1 increases as ω_t getting higher, meanwhile, the damping frequency ω_d provides a relatively wide bandwidth under the circumstance that α_1 and α_2 almost remain constants.

To deal with the error accumulation of the iteration process caused by the compressor mechanical structure or the temperature variation, the error correction law is proposed. Based on the compressor dynamics equation in (15), the error of ILC can be presented as

$$\dot{\lambda}(t) = \frac{T_e(t) - T_L(t) - J_m\dot{\omega}_m(t)}{K_t} \tag{30}$$

According to FIGURE 13, the error accumulation can be presented as

$$\lambda(t) = i_{qc}(t) - i_m(t) \tag{31}$$

Combing (28) and (29), the error of ILC can be rewritten as

$$\dot{\lambda}(t) = i_q^*(t) - i_m(t) - \lambda(t) - \frac{J_m\dot{\omega}_m(t)}{K_t} \tag{32}$$

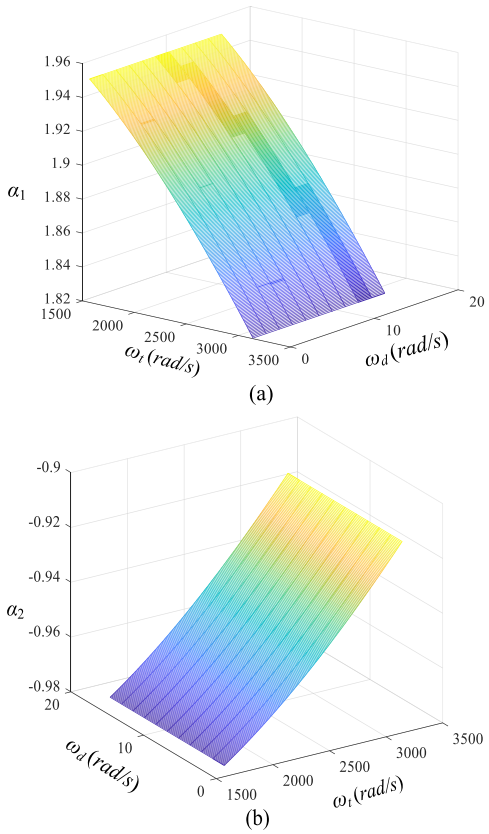

FIGURE 15. The coefficient variation with respect to ω_t and ω_d.

The error correction law can be obtained by integrating (30) as follows

$$\lambda(t) = \int \left(i_q^*(t) - i_m(t) - \lambda(t)\right)dt - \frac{J_m}{K_t}\omega(t) \tag{33}$$

According to (33), the numerical simulation results are shown in FIGURE 16 while the fluctuated load torque is implemented. It can be seen in FIGURE 16(a) that the error of ILC always exists and the error accumulation gradually increases from 0.58s during the compressor operating process, which is shown in FIGURE 16(b). The feedforward currents with and without the error correction law are both shown in FIGURE 15(c), the offset has been eliminated in $i_{qc}(t)$ when comparing with the generation of the conventional ILC method. The feedforward controller mainly deals with the fundamental component of speed ripple and the non-periodic component can be regulated by the speed controller.

IV. EXPERIMENTAL VERIFICATION

A. PREPARATION FOR THE EXPERIMENT

To verify the effectiveness of the proposed method, the experiments are performed on an air-conditioner system

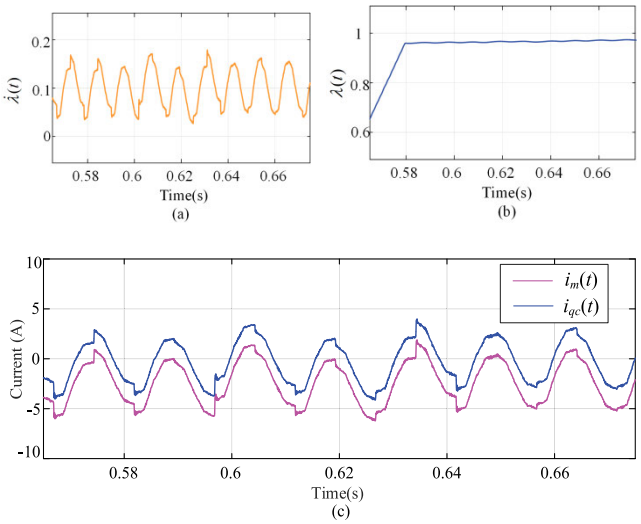

FIGURE 16. The numerical simulation results of the error correction law.

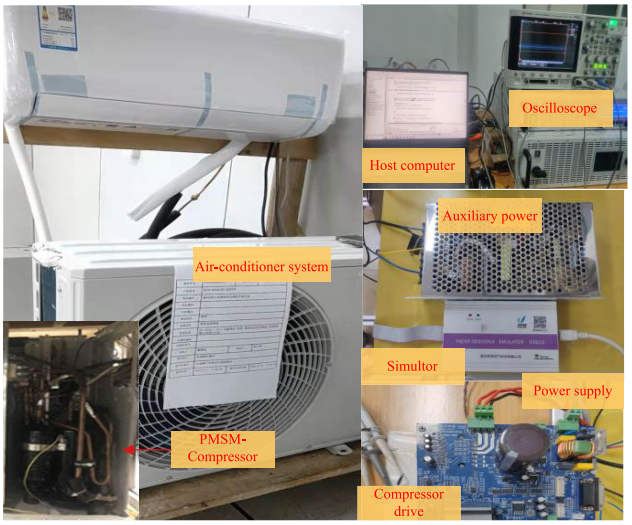

FIGURE 17. The platform of the PMSM based compressor system.

of 1 horsepower, and the platform is shown in FIGURE 17. The compressor is the core of the air- conditioner system, which is sealed in the cylinder filled with refrigerant. The compressor drive board is designed with a commercial power device IKCM30F60GA type intelligent power module (IPM), and is supplied by the auxiliary power. The waveforms of motor speed and current are acquired by the oscilloscope. The sampling frequency used in the experiment is 10kHz and matches with the switching frequency. The parameters of the PMSM-compressor are listed in Table 1. The initial

$$D(s) = \frac{-s\left(-\alpha_2 T_s^2 s^2 + (2\alpha_2 + \alpha_1) T_s s + 1 - \alpha_1 - \alpha_2\right)}{J_m \alpha_2 T_s^2 s^4 + \left(K_t K_{sp} \alpha_2 T_s^2 - J_m (2\alpha_2 + \alpha_1) T_s\right) s^3 + D_2 s^2 + D_1 s - K_t K_{si}(1 - \alpha_1 - \alpha_2)} \tag{27}$$

TABLE 1. Parameters of the Prototype.

Notation	Description	Value	Units
P	rated power	750	W
L_d	d-axis inductance	3.45	mH
L_q	q-axis inductance	6.02	mH
R_s	resistance	0.55	Ω
ψ_f	flux of rotor	0.093	Wb
P_p	poles pairs	4	
J_m	inertia	0.0013	kg·m^2

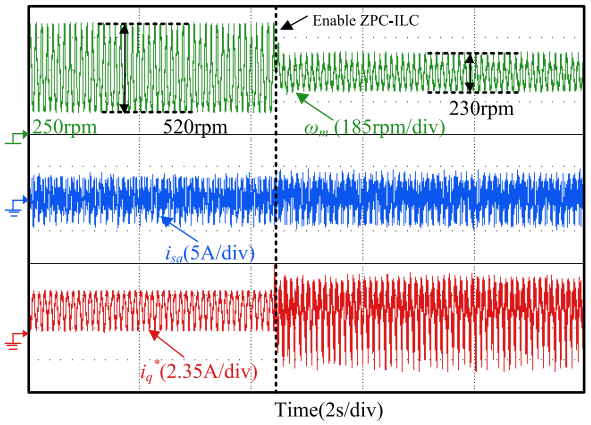

FIGURE 18. Experimental results for the proposed method at 600rpm.

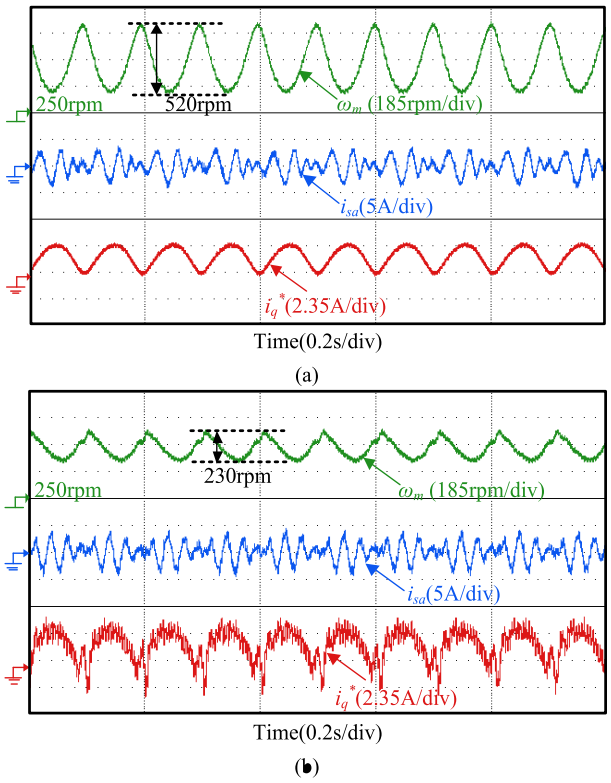

FIGURE 19. Comparison before and after enabling the proposed method in detail. (a) Zoom area without the suppression method. (b) With the proposed method.

parameters of the feedforward controller are chosen as α_1=1.85, α_2=-0.95.

B. EXPERIMENTAL RESULTS

FIGURE 18 presents the experimental results applying the proposed method when the compressor is operating at 600rpm (i.e., the mechanical frequency 10Hz). The waveforms in FIGURE 18 are the motor speed, phase current and q-axis reference current respectively. It can be seen that the speed ripple is serious under the low frequency operation, which reaches to 520rpm without any suppression method.

The enlarged waveforms before and after enabling the proposed method are presented in FIGURE 19. The speed ripple is 230rpm in can be FIGURE 19(a), which decreases by nearly 50% and the noise during the compressor operation can be simultaneously reduced. However, FIGURE 19(b) shows that the extra frequency components except for the fundamental one will be induced in the q-axis reference current by the feedforward term i_{qc}, which also reflects in the phase current i_{sa}, and this phenomenon is obvious as the compressor operating frequency getting higher.

The fast Fourier transform (FFT) results of the speed ripple are shown in FIGURE 20, where the fundamental one is the main component and the amplitude reaches to 235rpm without any suppression method. It can be seen from FIGURE 20(b) that both the 1st and 2nd components of speed ripple are effectively reduced as the proposed method is employed, which decreases by 63% comparing with that in FIGURE 20(a).

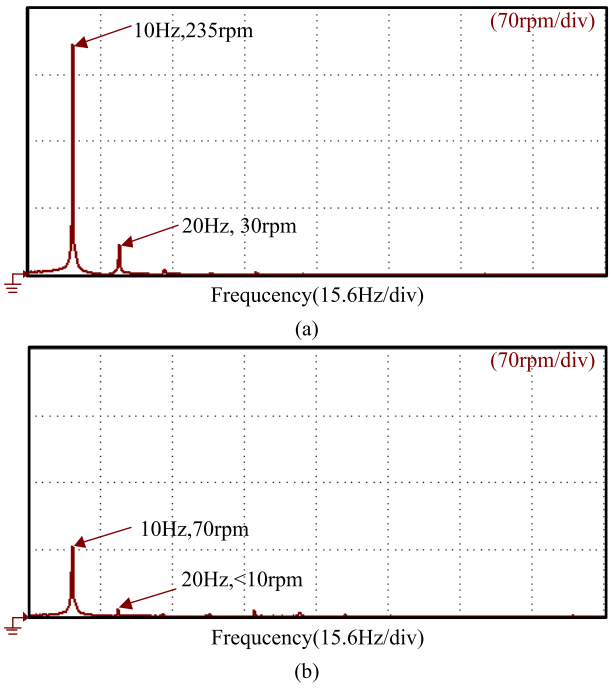

FIGURE 20. FFT results of the speed ripple before and after enabling the proposed method. (a) Without the suppression method. (b) With the proposed method.

TABLE 2. FFT results of speed ripple under different conditions.

	Speed ripple at 600rpm (10Hz)			Speed ripple at 900rpm (15Hz)			Speed ripple at 1200rp (20Hz)		
	10Hz	20Hz	30Hz	15Hz	30Hz	45Hz	20Hz	40Hz	60Hz
Without suppression (rpm)	235	30	10	200	23	10	180	15	10
Conventional ILC method (rpm)	165	25	10	152	15	10	130	15	10
Proposed method (rpm)	70	10	5	62.5	10	5	85	10	10

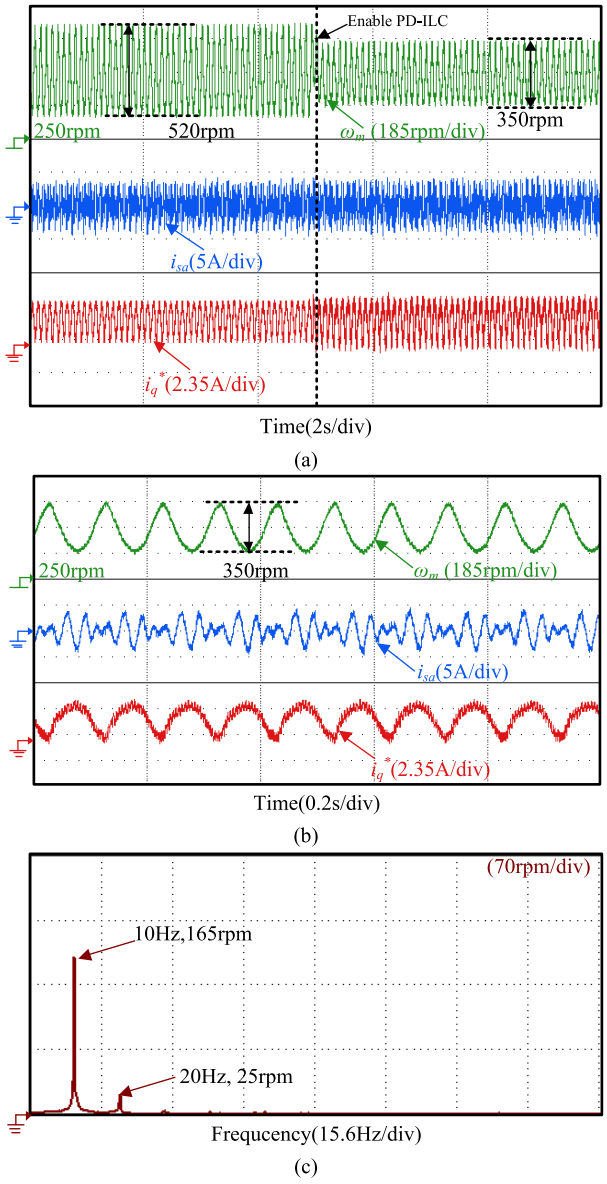

FIGURE 21. Experimental results for the conventional ILC method at 600rpm. (a) Comparison before and after enabling the method. (b) Zoom area with the ILC method. (c) FFT results of the speed ripple.

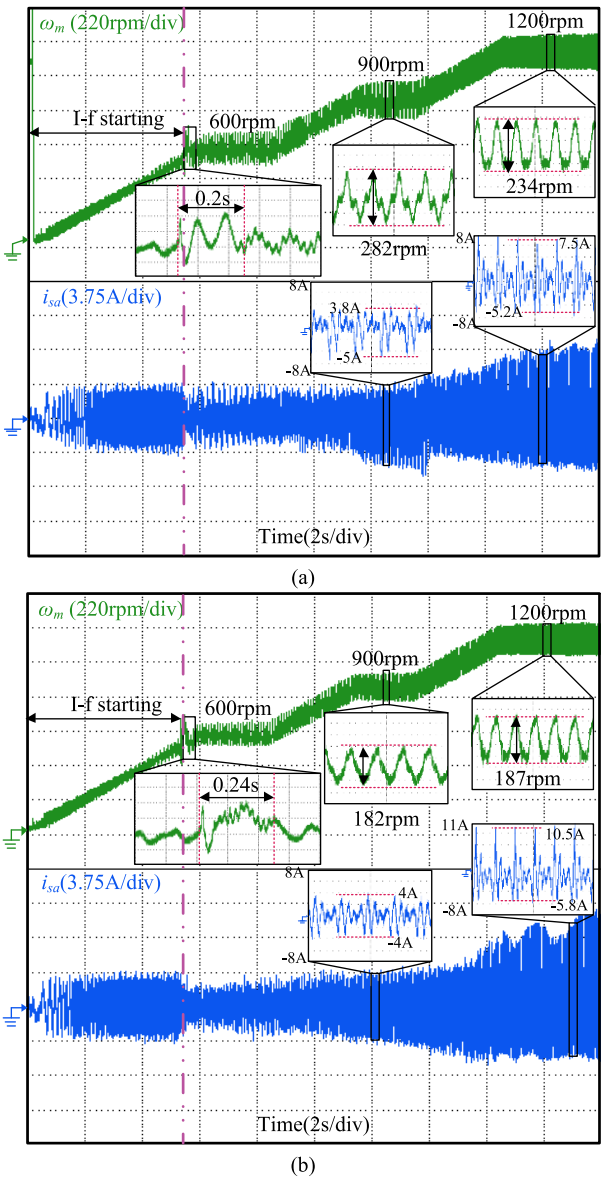

FIGURE 22. Waveforms of the motor speed and phase current during the starting up and accelerating process. (a) With the conventional ILC method. (b) With the proposed method.

The experimental results compared with the conventional ILC method are shown in FIGURE 21 as the compressor operating at 600rpm. It can be seen in FIGURE 21(b) that the speed ripple only reduces to 350rpm, which is nearly 1.5 times of that for the proposed method. From the FFT results shown in FIGURE 21(c), the amplitude of 1st and 2nd components are 165rpm and 25rpm, respectively, which indicates less effective for either the fundamental or

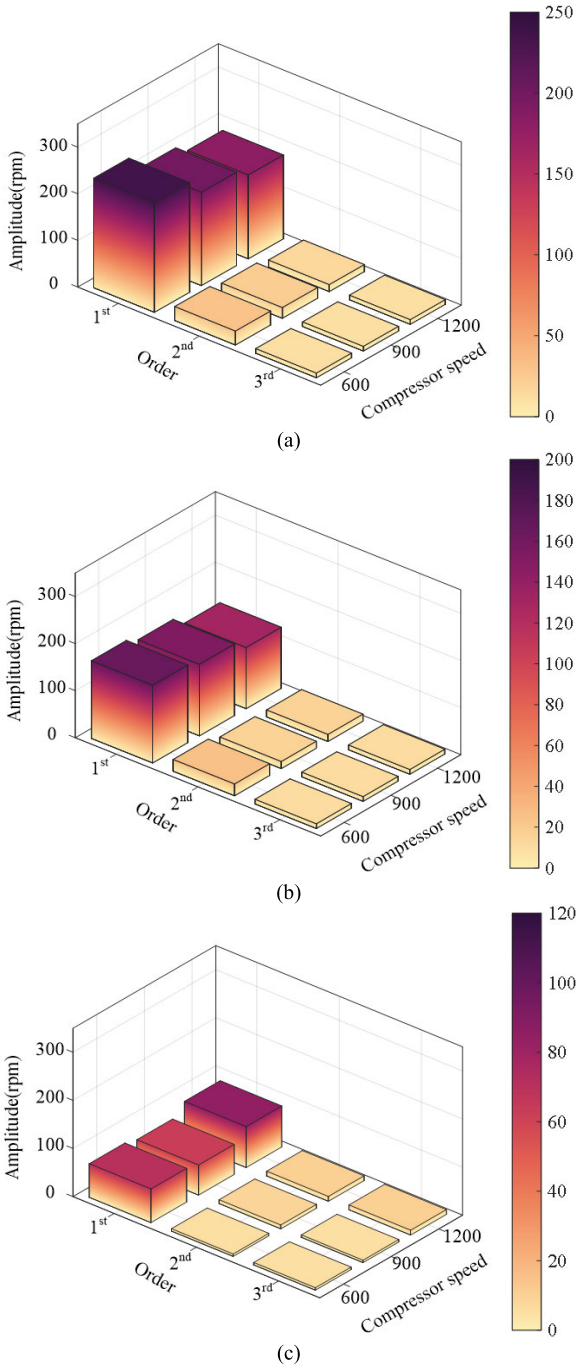

FIGURE 23. FFT result of speed ripple under different cases. (a) Without any suppression method. (b) With the conventional ILC method. (c) With the proposed method.

other components of the speed ripple within low frequency range.

Meanwhile, a more detailed explanation and comparison has been given for the conventional and proposed methods. To evaluate the dynamic performance of the two methods, FIGURE 22 shows the waveforms of the motor speed and phase current during the starting up and accelerating process (from 10Hz/600rpm to 20Hz/1200rpm). The I-f starting method is utilized for fast and reliable starting up due to the relatively light initial load for the compressor. The starting time is 5.2s with the ramp command, and then the compressor is operating under the sensorless control with the speed ripple suppression strategy. The enable time for the two algorithms are 0.2s and 0.24s respectively, which are labeled and zoomed in FUGURE 22. The enable time increases a little since the error correction law is included in the proposed method. The overshoot of speed waveform is also obvious at the enablement transient for the conventional ILC method.

It can be observed from FIGURE 22(a) that the speed ripples are 282rpm and 234rpm at 15Hz and 20Hz, respectively. However, the speed ripple reduces 34% and 21% while applying the proposed method, which are 182rpm and 187rpm at 15Hz and 20Hz shown in FIGURE 22(b). The suppression capability under the accelerating condition can be well maintained. In addition, the phase currents for both methods are presented in FIGURE 20. With the proposed method, the peak-peak value of i_{sa} reaches to 16.3A at 20Hz while it is 12.7A for the conventional ILC method, which means the satisfactory performance can be obtained at the cost of more current fluctuation is injection, and it should be noted that the peak-peak value is limited by the motor maximum current. The FFT results of the speed ripple under different cases are summarized in TABLE 2.

To further compare the performance of speed ripple suppression under different speed cases, the FFT analysis of the speed ripple under different compressor speed cases are given in FIGURE 23. As it can be seen in FIGURE 23(a) that the amplitude fluctuation of fundamental component is 235rpm under the speed of 600rpm, which also reveals that the speed ripple is a significant issue for lower frequency operation. As the conventional ILC method is applied, the amplitude of the fundamental component reduces to 165rpm as shown in FIGURE 23(b), which continuously decreases to 70rpm after applying the proposed method as shown in FIGURE 23(c). As the compressor speed getting higher (i.e., at 1200rpm), it can be seen in FIGURE 23(a) and (b) that the effects for speed ripple suppression are limited with the conventional ILC method, however, the speed ripple can be suppressed to 85rpm at 1200rpm while using the proposed method, which shows the significant advantage for the innovative approach. It can be concluded that the effect will be gradually weaken as the compressor operating in medium frequency, and the acceptable fluctuation mainly depends on the types of the single rolling rotor compressor.

V. CONCLUSION

This paper proposes a speed ripple suppression method through the zero-pole cancellation (ZPC) based iterative learning control (ILC) for the compressor drive system. A linear state observer in synchronous frame is applied to obtain the rotor position for sensorless control. In the proposed method, the torque ripple of the compressor is first

mathematically formulated in the frequency domain. Then, the speed ripples including each harmonic component are derived according to the compressor mechanical model. The poor performance of the conventional proportional-differential (PD) ILC is investigated from the aspect of poles effect of torque term. Inspired from this aspect, the poles' matching function is employed to extract the fundamental component from the torque term and decline the effect of disturbance term from zero-pole cancellation principle. Furthermore, the non-periodic disturbance caused by the operating frequency and temperature variation can be avoided by implementing the error correction law. Experimental results demonstrate the effectiveness of the proposed method in reducing speed ripples of the compressor drive without utilizing of motor electrical parameters.

It should be also pointed out that this paper focuses on the fundamental component suppression of the speed ripple, and then the bandwidth limitation of the current controller can be ignored. Therefore, the future work can focus on the high bandwidth current controller to extend speed harmonic compensation range. In the meanwhile, the performance of the proposed method can be improved by cooperating with the disturbance observer to deal with non-periodic disturbance.

APPENDIX

The coefficient matrix in (5) are presented as follows

$$\mathbf{A} = \begin{bmatrix} -\frac{R_s}{L_d} & \hat{\omega}_e \frac{L_q}{L_d} & \frac{1}{L_d} & 0 \\ -\hat{\omega}_e \frac{L_d}{L_q} & -\frac{R_s}{L_q} & 0 & \frac{1}{L_q} \\ 0 & 0 & 0 & 0 \\ 0 & 0 & 0 & 0 \end{bmatrix} \tag{A1}$$

$$\mathbf{B} = \begin{bmatrix} \frac{1}{L_d} & 0 \\ 0 & \frac{1}{L_q} \\ 0 & 0 \\ 0 & 0 \end{bmatrix} \tag{A2}$$

$$\mathbf{C} = \begin{bmatrix} 1 & 0 & 0 & 0 \\ 0 & 1 & 0 & 0 \end{bmatrix} \tag{A3}$$

The coefficient D_1 and D_2 in (27) are presented as follows

$$D_1 = K_{sp} K_t \left(\alpha_1 + \alpha_2 - 1\right) - K_{si} K_t T_s \left(\alpha_1 + 2\alpha_2\right) \tag{A4}$$

$$D_2 = J_m \left(\alpha_1 + \alpha_2 - 1\right) + K_t T_s \times \left(\alpha_2 K_{si} T_s - 2\alpha_2 K_{sp} - \alpha_1 K_{sp} - 1\right) \tag{A5}$$

REFERENCES

[1] S. Ye and X. Yao, "A modified flux sliding-mode observer for the sensorless control of PMSMs with online stator resistance and inductance estimation," *IEEE Trans. Power Electron.*, vol. 35, no. 8, pp. 8652–8662, Aug. 2020.

[2] C. Wu, Y. Zhao, and M. Sun, "Enhancing low-speed sensorless control of PMSM using phase voltage measurements and online multiple parameter identification," *IEEE Trans. Power Electron.*, vol. 35, no. 10, pp. 10700–10710, Oct. 2020.

[3] Q. Yang, K. Mao, S. Zheng, C. Zhou, and Q. Zhong, "Position sensorless drive with online parameters estimation for magnetic suspension centrifugal compressor," *IEEE Trans. Power Electron.*, vol. 38, no. 8, pp. 9384–9394, Aug. 2023.

[4] Z. Hao, Y. Yang, Y. Tian, Y. Gong, C. Zhang, H. Song, Z. Hao, and J. Zhang, "Phase lead compensation of a phase-locked loop in an IPMSM for air-conditioner compressors," *IEEE Trans. Energy Convers.*, vol. 36, no. 2, pp. 1090–1100, Jun. 2021.

[5] A. Dianov and A. Anuchin, "Offline measurement of stator resistance and inverter voltage drop using least squares," *IEEE Access*, vol. 11, pp. 17053–17065, 2023.

[6] Y. Li, Y. Pan, P. Ba, S. Wu, and J. Chen, "Fault feature extraction method of reciprocating compressor valve based on SPA-MF," *IEEE Access*, vol. 10, pp. 127182–127191, 2022.

[7] G. Liu, G. Xu, W. Zhao, X. Du, and Q. Chen, "Improvement of torque capability of permanent-magnet motor by using hybrid rotor configuration," *IEEE Trans. Energy Convers.*, vol. 32, no. 3, pp. 953–962, Sep. 2017.

[8] C. Xia, B. Ji, and Y. Yan, "Smooth speed control for low-speed high-torque permanent-magnet synchronous motor using proportional–integral–resonant controller," *IEEE Trans. Ind. Electron.*, vol. 62, no. 4, pp. 2123–2134, Apr. 2015.

[9] J. Lara, J. Xu, and A. Chandra, "Effects of rotor position error in the performance of field-oriented-controlled PMSM drives for electric vehicle traction applications," *IEEE Trans. Ind. Electron.*, vol. 63, no. 8, pp. 4738–4751, Aug. 2016.

[10] J. Huo, N. Zhao, R. Gao, G. Wang, G. Zhang, and D. Xu, "Torque ripple compensation with anti-overvoltage for electrolytic capacitorless PMSM compressor drives," *IEEE J. Emerg. Sel. Topics Power Electron.*, vol. 10, no. 5, pp. 6148–6159, Oct. 2022.

[11] Y. Bai, N. Zhao, G. Wang, G. Zhang, and D. Xu, "Speed ripple suppression of reduced DC-link capacitance IPMSM drives for air-conditioning applications," in *Proc. IEEE Appl. Power Electron. Conf. Expo. (APEC)*, Anaheim, CA, USA, Mar. 2019, pp. 3039–3044.

[12] K. Wang, Z. Y. Gu, Z. Q. Zhu, and Z. Z. Wu, "Optimum injected harmonics into magnet shape in multiphase surface-mounted PM machine for maximum output torque," *IEEE Trans. Ind. Electron.*, vol. 64, no. 6, pp. 4434–4443, Jun. 2017.

[13] J. Qu, J. Jatskevich, C. Zhang, and S. Zhang, "Torque ripple reduction method for permanent magnet synchronous machine drives with novel harmonic current control," *IEEE Trans. Energy Convers.*, vol. 36, no. 3, pp. 2502–2513, Sep. 2021.

[14] C. Lai, G. Feng, K. L. V. Iyer, K. Mukherjee, and N. C. Kar, "Genetic algorithm-based current optimization for torque ripple reduction of interior PMSMs," *IEEE Trans. Ind. Appl.*, vol. 53, no. 5, pp. 4493–4503, Sep. 2017.

[15] W. Qian, S. K. Panda, and J. X. Xu, "Speed ripple minimization in PM synchronous motor using iterative learning control," *IEEE Trans. Energy Convers.*, vol. 20, no. 1, pp. 53–61, Mar. 2005.

[16] G. Feng, C. Lai, and N. C. Kar, "A closed-loop fuzzy-logic-based current controller for PMSM torque ripple minimization using the magnitude of speed harmonic as the feedback control signal," *IEEE Trans. Ind. Electron.*, vol. 64, no. 4, pp. 2642–2653, Apr. 2017.

[17] S. Wang, G. Zhang, Q. Wang, D. Ding, G. Bi, B. Li, G. Wang, and D. Xu, "Torque disturbance compensation method based on adaptive Fourier-transform for permanent magnet compressor drives," *IEEE Trans. Power Electron.*, vol. 38, no. 3, pp. 3612–3623, Mar. 2023.

[18] W. Huang, W. Hua, X. Zhu, Y. Fan, and M. Cheng, "Comparison of cogging torque compensation methods for a flux-switching permanent magnet motor by harmonic current injection and iterative learning control," in *Proc. Int. Conf. Electr. Mach. (ICEM)*, vol. 1, Aug. 2020, pp. 1971–1977.

[19] Y. Gu, L. Quan, and Z. Xiang, "Minimization the torque ripple of flux-switching permanent magnet motor based on iterative learning control," in *Proc. 17th Int. Conf. Electr. Mach. Syst. (ICEMS)*, Oct. 2014, pp. 1985–1989.

[20] P. Kshirsagar, R. P. Burgos, A. Lidozzi, J. Jang, F. Wang, D. Boroyevich, and S.-K. Sul, "Implementation and sensorless vector-control design and tuning strategy for SMPM machines in fan-type applications," in *Proc. Conf. Rec. IEEE Ind. Appl. Conf., 41st IAS Annu. Meeting*, vol. 4, Tampa, FL, USA, Oct. 2006, pp. 2062–2069.

[21] R. P. Burgos, P. Kshirsagar, A. Lidozzi, F. Wang, and D. Boroyevich, "Mathematical model and control design for sensorless vector control of permanent magnet synchronous machines," in *Proc. IEEE Workshops Comput. Power Electron.*, Troy, NY, USA, Jul. 2006, pp. 76–82.

YAN WANG was born in Heilongjiang, China, in 1988. He received the B.Sc. and master's degrees in electrical engineering from Harbin University of Science and Technology, Heilongjiang, in 2014, and the Ph.D. degree in electrical engineering from the College of Electrical Engineering, Zhejiang University, Hangzhou, China, in 2020. Since 2021, he has been with the College of Information Science and Engineering, Zhejiang Sci-Tech University, China, where he is currently a Lecturer. His current research interest includes the multiphase machine design and control technique.

SHENGHUI DENG was born in Henan, China, in 2002. He received the B.Eng. degree in electric engineering from Zhejiang Sci-Tech University, Zhejiang, China, in 2023. He is currently pursuing the M.Eng. degree in control science and engineering with Zhejiang Sci-Tech University, Hangzhou, China. His current research interest includes motor design and motor control. He is conducting research on multiphase permanent magnet assisted synchronous reluctance motors.

WENQI LU (Member, IEEE) received the B.S. degree in power electronics and power drives from Zhejiang Ocean University, Zhejiang, China, in 2005, and the Ph.D. degree in power electronics and power drives from Nanjing University of Aeronautics and Astronautics, Nanjing, China, in 2011.

From 2014 to 2017, he was a Postdoctoral Researcher with the Department of Electrical Engineering, Zhejiang University, Zhejiang. From 2017 to 2018, he was a Guest Researcher with the Department of Energy Technology, Aalborg University, Aalborg, Denmark. He is currently an Associate Professor with the Faculty of Mechanical Engineering and Automation, Zhejiang Sci-Tech University, Zhejiang. His research interests include the control of electric machines and mechatronic systems and their application in robot and intelligent manufacturing equipment.